Simple excision of a black hole in 3+1 numerical relativity

Miguel Alcubierre and Bernd Brügmann
Max-Planck-Institut für Gravitationsphysik, Albert-Einstein-Institut, Am Mühlenberg 1, 14476 Golm, Germany
(Received 6 September 2000; published 5 April 2001)

We describe a simple implementation of black hole excision in 3+1 numerical relativity. We apply this technique to a Schwarzschild black hole with octant symmetry in Eddington-Finkelstein coordinates and show how one can obtain accurate, long-term stable numerical evolutions.

DOI: 10.1103/PhysRevD.63.104006 PACS number(s): 04.25.Dm, 04.30.Db, 95.30.Sf, 97.60.Lf

The simulation of a black hole inspiral collision is one of the most important open problems facing numerical relativity. Traditional techniques using singularity avoiding slicings will not be able to follow such a collision since problems associated with the stretching of the slice typically cause simulations to crash or to become extremely inaccurate in time scales far shorter than the orbital time scale. Black hole excision techniques (also known as ''apparent horizon boundary condition'' [1,2]) appear to be the most promising way of eliminating the problem of the slice stretching, thus in principle allowing numerical simulations to follow the inspiral from well separated holes through the merger and the ring-down phase.

Black hole excision was first attempted successfully by Seidel and Suen in spherical symmetry [1], and was later studied in more detail by Anninos *et al.* [2]. However, the original idea is older, and Thornburg [3,4] has attributed it to a suggestion by Unruh from 1984. The idea consists of two parts: First, one places a boundary inside the black hole and excises its interior from the computational domain; second, one uses a shift vector that keeps the horizon roughly in the same coordinate location during the evolution (''horizon tracking,'' see [4]). Since no information can leave the interior of the black hole, excision should have no effect on the physics outside. Ideally, one would like to know the position of the event horizon which marks the true causal boundary, but the global character of its definition means that in principle one can only locate it once the whole evolution of the spacetime is known. The apparent horizon, on the other hand, can be located on every time slice and is guaranteed to be inside the event horizon. In practice one therefore needs to find the apparent horizon and excise a region contained inside it.

Though black hole excision has been successful in spherical symmetry [1,2,5–10], it has been difficult to implement with a 3+1 approach in three-dimensions (3D) [11–14], where instabilities typically plague the evolutions (but some progress has been made, see [15,16]). Black hole excision using a characteristic formulation, on the other hand, has been very successful in 3D, allowing stable evolutions of perturbed black holes for thousands of M's [17]. However, such characteristic formulations are likely to have problems with the development of caustics in the case of extremely distorted or colliding black holes, so the search for a stable 3+1 excision implementation is still of great importance.

Here we present a 3+1 approach to black hole excision in 3D that has allowed us to obtain long-term stable, accurate evolutions of a single black hole spacetime. These results are currently limited to simulations in octant symmetry as discussed below.

I. SIMPLE BLACK HOLE EXCISION

Though conceptually simple, black hole excision in 3D is a complicated problem numerically. First, one has to cut a hole in the computational domain that has a spherical topology and is therefore not well adapted to the Cartesian coordinates typically used. Second, one has to apply some condition at the boundary of the excised region that is stable and respects the causality of the physical system. As the excised region is inside a black hole, no boundary condition should be needed since all the information required to update the boundary comes from outside the excised region. However, achieving this ''boundary without a boundary condition'' (BWBC) [1,7] in 3D is difficult, particularly if one uses a formulation of the evolution equations that is not hyperbolic. The way this problem is usually approached is by using ''causal differencing'' [1,2] or ''causal reconnection'' [18], where the computational molecules are adapted to follow the causal structure. The mixture of these issues makes it difficult in practice to identify what particular element of an algorithm is responsible for causing a numerical simulation to go unstable.

In our approach we have simplified the algorithm as much as possible, separating out what we believe is essential to the excision problem. Our algorithm is based on the following simplifications:

Excise a region adapted to Cartesian coordinates, i.e. excise a cube contained inside the horizon.

Do not attempt to satisfy the BWBC ideal, and use instead a simple but stable boundary condition at the excision boundary.

Do not use causal differencing. Use instead centered differences in all terms except the advection terms on the shift (terms that look like $\beta^i \partial_i$). For these terms use upwind along the shift direction (we use the standard 1D second-order upwind stencil in each of the Cartesian coordinate directions based on the sign of the corresponding shift component at each point). This is very important, as it is the only place where any information about causality (i.e. the direction of the shift) enters our scheme. Using a centered approximation for these terms results in an unstable scheme.

One can worry that excising a cube will introduce arti-

facts into the evolution, but as long as the boundary condition used at the sides of the cube is consistent those artifacts will converge away with increased resolution. Similarly, one can argue that applying a boundary condition instead of using causal differencing is inconsistent with the physics, but since this condition is applied well inside the horizon, any error introduced is unlikely to propagate outside the hole.

II. STATIC BLACK HOLE SPACETIME

As the first test of our excision algorithm we have considered a single static black hole written in ''3+1 Eddington-Finkelstein''(EF) coordinates. These 3+1 EF coordinates are a simple transformation of the standard ingoing EF coordinates [19] to a 3+1 form. The resulting metric has no coordinate singularities, penetrates the event horizon, reaches the physical singularity, and is manifestly time independent. This makes it ideal for excision tests where one can excise the physical singularity and try to keep the numerical evolution stable and close to static. The 3+1 EF metric has the form

$$ds^2 = -(1-2M/r)dt^2 + (4M/r)dtdr + (1+2M/r)dr^2 + r^2 d\Omega^2, \tag{1}$$

with M the black hole mass and $d\Omega$ the solid angle element. From this metric one can read the values of the 3-metric, lapse and shift. The extrinsic curvature can then be obtained in a straightforward way.

III. EVOLUTION EQUATIONS

Formulation. We comment briefly on the formulation used for the simulations described below. Our simulations have been performed using a formulation of the 3+1 evolution equations developed by Baumgarte and Shapiro [20] (BS), based on previous work of Shibata and Nakamura [21] (SN). The motivation for using this BSSN formulation comes from the fact that it has shown remarkable stability properties when compared to the Arnowitt-Deser-Misner (ADM) formulation [22] in a wide range of numerical simulations [20,23–28].

The BSSN variables are defined in terms of the spatial metric γ_{ij} and the extrinsic curvature K_{ij} as $\phi = \ln(\det \gamma_{ij})/12$, $\tilde{\gamma}_{ij} = e^{-4\phi}\gamma_{ij}$, $\mathrm{tr}\, K = \gamma^{ij}K_{ij}$, $\tilde{A}_{ij} = e^{-4\phi}(K_{ij} - \gamma_{ij}\,\mathrm{tr}\, K/3)$, and $\tilde{\Gamma}^i = \tilde{\gamma}^{jk}\Gamma^i_{jk}$ (note that $\det \tilde{g} = 1$ and $\mathrm{tr}\,\tilde{A} = 0$). See [20] for the explicit form of the evolution equations, and [28] for an analysis that indicates why the BSSN formulation should be superior to ADM at least for linearized perturbations of flat space.

In order to obtain the stable evolutions described below, we have found it necessary to add the following ingredients to the BSSN formulation:

(1) As discussed in [29], we actively force the trace of the conformal-traceless extrinsic curvature $\tilde{A}_{ij}$ to remain zero during our simulations by subtracting it after each time step.

(2) We use the independently evolved ''conformal connection functions'' $\tilde{\Gamma}^i$ only in terms where derivatives of these functions appear. Whenever these functions are undifferentiated, we recompute them from the conformal Christoffel symbols. We have found this to be very important to achieve long-term stability, but at the moment we lack a theoretical understanding as to why this is so.

Slicing conditions. As a first approach to evolving the solution described above, one could think of using the exact value of the lapse. It turns out that it is difficult to keep the evolution stable if the lapse is not allowed to adapt to the (numerically induced) evolution of other dynamical quantities, particularly the trace of the extrinsic curvature. In order to obtain stable evolutions we have found it crucial to use a ''live'' slicing condition. What is required is a slicing condition that is well adapted to the exact solution in the sense that for this solution it recovers the exact lapse. For this we start from the Bona-Massó family of slicing conditions [30]

$$\partial_t \alpha = -\alpha^2 f(\alpha)\,\mathrm{tr}\, K, \tag{2}$$

with $f(\alpha) > 0$. As it is, this condition does not reproduce our exact solution for which $\mathrm{tr}\, K \neq 0$, but $\partial_t \alpha = 0$. However, one can easily see that for zero shift Eq. (2) implies $\partial_t \alpha \propto \partial_t(\det g)$. For this to hold also with non-zero shift Eq. (2) must be generalized to

$$\partial_t \alpha = -\alpha f(\alpha)[\alpha\,\mathrm{tr}\, K - \nabla_i \beta^i]. \tag{3}$$

For any static solution Eq. (3) implies $\partial_t \alpha = 0$.

Another natural slicing condition to consider is $\partial_t \mathrm{tr}\, K = 0$. For initial data with $\mathrm{tr}\, K = 0$ this condition leads to maximal slicing, but $\partial_t \mathrm{tr}\, K = 0$ is a gauge choice that can be made in general, even if $\mathrm{tr}\, K \neq 0$, as is the case for the constant time slices of the black hole in EF coordinates. This ''K freezing'' condition leads to an elliptic equation for the lapse,

$$\Delta \alpha - \alpha K_{ij} K^{ij} - \beta^i \nabla_i \mathrm{tr}\, K = 0. \tag{4}$$

In the numerical implementation, we solve this equation for the lapse but we hold $\mathrm{tr}\, K$ constant in time by hand. In [27] in the context of the evolution of strong waves we have found that otherwise a drift away from the initial value due to numerical errors can lead to an instability. Such drifts were one of the reasons that led us to consider trace-split formulations like BSSN, because here $\mathrm{tr}\, K$ is evolved as an independent variable which makes it trivial to enforce $\partial_t \mathrm{tr}\, K = 0$.

Shift conditions. In contrast to the experience with the lapse, we have found that using a static (exact) shift does allow us to get long-term stable evolutions. However, this is not useful in general, so we have considered also live shift conditions. Live shifts have been studied before for black hole spacetimes in [12], where a minimal distortion shift condition [31] led to limited stability ($t \sim 100M$) for a single excised black hole.

In our case a good choice was a conformal version of the 3-harmonic shift [32]. 3-harmonic shifts play a natural role in mixed elliptic-hyperbolic systems [33]. The condition we impose in the BSSN system is $\partial_t \tilde{\Gamma}^k = 0$ (''Gamma freezing'' condition, note that $\tilde{\Gamma}^k \neq 0$), or

$$\tilde{\gamma}^{jk}\partial_j\partial_k\beta^i+\frac{1}{3}\tilde{\gamma}^{ij}\partial_j\partial_k\beta^k-\tilde{\Gamma}^j\partial_j\beta^i+\frac{2}{3}\tilde{\Gamma}^i\partial_j\beta^j+\beta^j\partial_j\tilde{\Gamma}^i$$

$$-2\tilde{A}^{ij}\partial_j\alpha-2\alpha\left(\frac{2}{3}\tilde{\gamma}^{ij}\partial_j\mathrm{tr}K-6\tilde{A}^{ij}\partial_j\phi-\tilde{\Gamma}^i_{jk}\tilde{A}^{jk}\right)=0. \tag{5}$$

As mentioned before, $\partial_k\tilde{\Gamma}^i$ is computed from the independent variable $\tilde{\Gamma}^i$, in other terms we use $\tilde{\Gamma}^i=\tilde{\gamma}^{jk}\tilde{\Gamma}^i_{jk}$ [notice that the momentum constraint was used to replace $\partial_j\tilde{A}^{ij}$ in Eq. (5)]. Equation (5) is an elliptic equation for the shift vector. For the solution of Eqs. (4) and (5) we have used the multi-grid solver from BAM, a bifunctional adaptive mesh code [34]. As in the case of K freezing, we explicitly hold the value of $\tilde{\Gamma}^i$ constant in time in order to prevent this quantity from drifting due to numerical errors. As shown in Sec. IV, allowing $\tilde{\Gamma}^i$ to drift results in an unstable evolution.

We have also looked at shift prescriptions given by evolution equations instead of elliptic conditions. One way to do this is to transform an elliptic equation into a parabolic one by making $\partial_t\beta^i$ proportional to the given elliptic operator (''driver'' conditions, see [35]). As an example we considered the following evolution equation for the shift obtained from the Gamma freezing condition (a ''Gamma driver'' condition)

$$\partial_t\beta^i=k\,\partial_t\tilde{\Gamma}^i \quad (k>0). \tag{6}$$

Boundary conditions. There are two very different boundaries to consider in our simulations: the outer boundary of the numerical grid, and the inner boundary of the excised region. In principle there should be a rigorous treatment of numerical boundaries at finite radii (starting e.g. from [36], the first analytic treatment of the initial boundary value problem). Here we are looking for simple numerical methods that are sufficient for the evolution of excised black holes.

At the outer boundary we have attempted to keep all fields equal to their exact values, but have found that this introduces late time instabilities. Using a live boundary condition allows us to eliminate these instabilities. The boundary condition we use is a radiative boundary condition applied to the difference between a given variable and its exact value: $f-f_{\mathrm{exact}}=u(r-t)/r$. We apply this condition to all fields (even to the lapse and shift in the case of the algebraic gauge conditions) *except* the $\tilde{\Gamma}^i$ which we leave fixed to their exact values at the boundary. Applying this condition to the $\tilde{\Gamma}^i$ causes a drift away from the exact solution that eventually crashes the simulation (the origin of this drift is not well understood, but it seems to be related to the shift choice and is not present if one uses the Gamma driver shift described above).

As to what boundary condition to use at the sides of the excision cube, we have experimented with many different conditions and have finally settled on one that simply copies the time derivative of every field at the boundary from its value one grid-point out along the normal direction to the cube (at edges and corners we define the normal direction as the diagonal). This condition is perfectly consistent with evolving a static solution, where the time derivatives are supposed to be zero. Even in a dynamical situation, this condition is still consistent with the evolution equations since it is equivalent to just calculating the source term one grid point away. This means that our boundary condition should introduce a first order error, but as mentioned above, we do not expect this error to affect the solution outside the horizon. One could in principle argue that nothing prevents gauge modes and constraint violating modes from propagating outside the horizon, thus spoiling the second order convergence of the exterior scheme. We have looked carefully at the convergence of our simulations, and have found no evidence that this happens in practice.

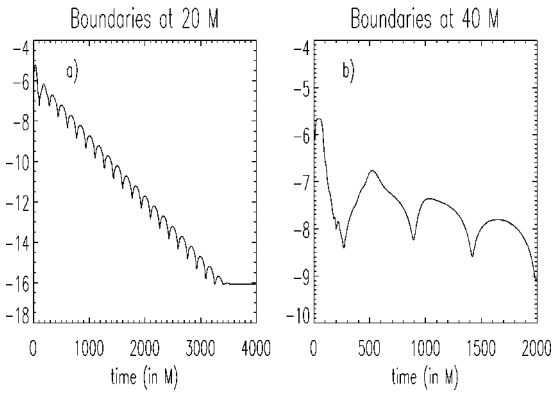

FIG. 1. Log plot of rms of the change in the lapse; $\Delta x=0.4$, $\Delta t=0.1$. (a) 53^3 grid points, boundary at $20M$. (b) 103^3 grid points, boundary at $40M$.

IV. NUMERICAL RESULTS

We now present some results of our numerical simulations. As discussed above, our simulations have been done with a live lapse condition, and we have considered both a static shift, and several live shift conditions. In our runs we have always taken $M=1$, so the horizon is a sphere of radius $r=2$, and we excise a cube of side 1 (we have in fact also excised cubes of different size, but the results discussed below are not affected by this). The numerical integration is carried out using the so-called iterative Crank-Nicholson scheme with 3 iterations (counting the initial Euler step as iteration 1). Because of the spherical symmetry of the problem typically only one octant was evolved (with positive x, y, and z). However, as discussed at the end of this section, an unstable mode appears when the same simulations are performed on the corresponding full grids.

Static shift. We first consider the case when the shift remains equal to its exact value. Figure 1 shows a log plot of the root mean square (rms) of the change in the lapse between consecutive time steps for two simulations using slicing condition (3) with $f=1/\alpha$ (''1+log'' slicing [29,37]), a grid spacing $\Delta x=0.4$, and a time step $\Delta t=0.1$. Figure 1(a) shows the results of a simulation using 53^3 grid points, with the outer boundaries at $20M$. The change in the lapse drops as an exponentially damped oscillation until at $t\sim 3500M$ it reaches the level of round-off error (10^{-16}) and settles down

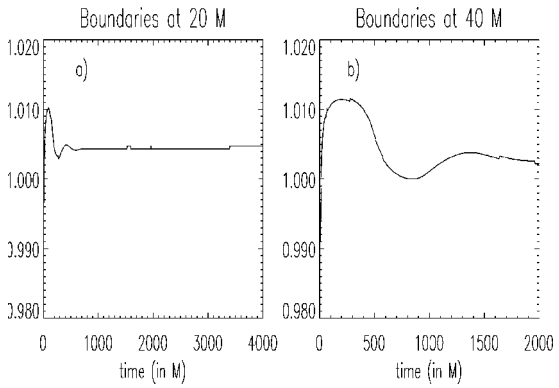

FIG. 2. Evolution of horizon mass for the same simulations.

(other functions show a similar behavior). The evolution was stopped at $t=4000M$, but it is clear that it could have continued. Figure 1(b) shows a simulation with the same resolution, but using 103^3 grid points, with the outer boundaries now at $40M$. The simulation goes past $t\sim 2000M$, and seems to have settled on an exponentially decaying oscillating pattern. (This simulation took 100 hours running on 16 processors of an Origin 2000 SGI machine. If the pattern continues, round-off error level would be reached by $t\sim 12000M$, requiring another 500×16 hours of computer time.) The most obvious differences between the run with the boundaries at $20M$ and that with the boundaries at $40M$ is the fact that the period of the oscillations increases and the rate of decay decreases. The period increases by a factor of 3.4 as we double the distance to the outer boundaries, so the oscillation time scale is not given directly by the light travel time from the boundary (which would approximately double). We do not know exactly what fixes this time scale, but the fact that when we look at individual metric components we see that the oscillations behave like standing waves (and not traveling pulses) would seem to indicate that we are looking at different modes of oscillation of the whole system (interior plus boundaries).

These simulations are not only stable for very long times, they are also exceedingly accurate. We have located the apparent horizon every 50 time steps (using the 3D finder described in [38]), measured its area A and computed its mass $M=\sqrt{A/(16\pi)}$. Figure 2 shows the behavior of the horizon mass as a function of time. In both cases, after an initial transient, the mass settles on a stationary value with an error of less than 1%.

In Fig. 3 we consider the convergence of our simulations by looking at the late time value of the Hamiltonian constraint along the x axis for simulations with 28^3, 53^3, and 103^3 grid points and resolutions of $\Delta x=0.4,0.2,0.1$ respectively (boundaries at $10M$). The Hamiltonian constraint for the higher resolution runs has been multiplied by factors of 4 and 16. The fact that the three lines coincide indicates second order convergence.

Elliptic shifts. We now consider results with elliptic shifts, such as those that we expect will be needed in a 3D black hole merger simulation. Figure 4 shows two stable and three unstable runs up to $t=400M$, and Fig. 5 shows those three runs that lasted longer up to $t=3000M$. Second order con-

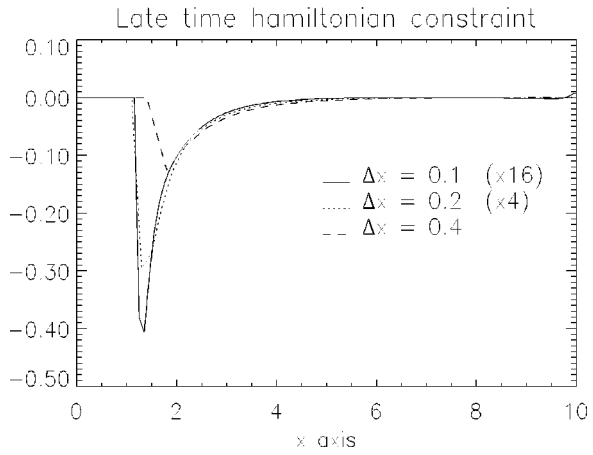

FIG. 3. Late time Hamiltonian constraint for runs with different resolutions. The values for the higher resolution runs were multiplied by factors of 4 and 16.

vergence has been checked using two grids with 19^3 and 35^3 points with the outer boundary at $7M$. For $1+\log$ slicing a radiative boundary condition is applied to the lapse, while lapse and shift for the elliptic conditions are held fixed at the exact values.

Stable runs are obtained for Gamma freezing shift with either $1+\log$ or K freezing slicings. Referring to Figs. 4 and 5, for $1+\log$ slicing $\Delta\alpha_{\rm rms}$ falls below 10^{-16} at $t\sim 1500M$ after four oscillations (run 1), while for K freezing there are more than fifteen oscillations, which damp out at around 10^{-10} followed by a straight line decay (run 2).

The $1+\log$, Gamma freezing run becomes unstable if the boundary values of all fields are static (run 3, crashing at t

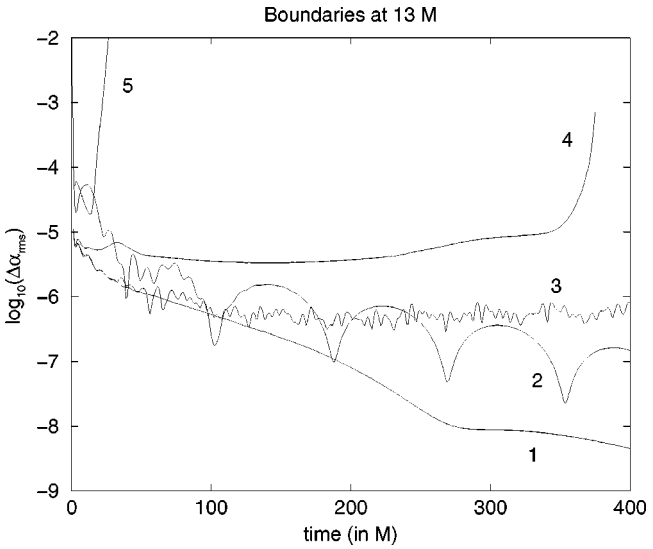

FIG. 4. Log plot of rms of the change in the lapse for different lapse and shift combinations involving elliptic conditions; $\Delta x=0.4$, $\Delta t=0.1$, 35^3 points, boundary at $13M$. Run 1: stable (Γ freezing without drift, $1+\log$); run 2: stable (Γ freezing without drift, K freezing without drift); run 3: unstable (Γ freezing without drift, $1+\log$, static outer boundaries); run 4: unstable (Γ freezing with drift, $1+\log$); run 5: unstable (minimal distortion, $1+\log$).

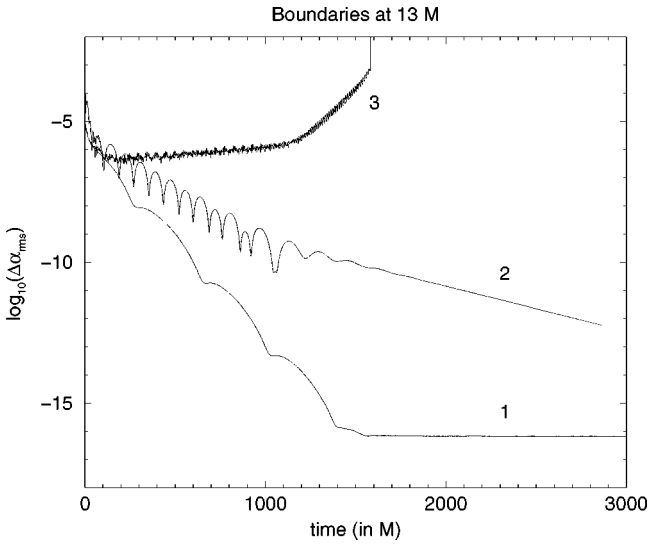

FIG. 5. Runs 1, 2, and 3 of Fig. 4 for run times of up to $t=3000M$.

$\sim 1500M$, Fig. 4, or if $\partial_t \tilde{\Gamma}^i = 0$ is not set to zero identically and is allowed to drift because of numerical errors (run 4, crashing at $375M$). We also tested $1+\log$ slicing with a minimal distortion shift [31] computed from the ADM variables, but this run fails already at $27M$ (run 5).

Algebraic shifts. Finally, we consider a simulation using $1+\log$ slicing and a Gamma driver shift with $k=0.1$. Figure 6 shows the rms of the change in the lapse and the horizon mass for a simulation with $\Delta x=0.4$, $\Delta t=0.1$ and 53^3 grid points. After $t\sim 2500M$ the solution becomes static up to round-off error.

Discussion. The above results demonstrate that stable 3D black hole runs can be obtained with the simple excision technique that we introduced in this paper, with a variety of different gauge conditions. However, repeating these runs on a full grid as opposed to just one octant, with otherwise identical parameters, uncovers an unstable mode. Figure 7 shows as an example the situation for $1+\log$ slicing and static shift, although the problem appears for all the gauge conditions considered here. Tracing the growth of the unstable mode back in time suggests that it has started as numerical round-off error of around 10^{-14} at $t=0$. Increasing the grid resolution appears to have no significant effect on the growth rate of the unstable mode, but the simulation now crashes slightly sooner. However, we do see good second order convergence at early times, before the instability becomes apparent. The situation does not improve if we impose the exact data at the excision boundary (imposing exact data at the excision boundary in octant mode works well and leads to stable simulations). Also, the presence of a horizon does not seem to be the cause of the problem since when we excise a cube that contains the horizon, as opposed to being contained by it, the instability is still present although it becomes somewhat milder (not surprising since we have excised a region with stronger data). While the achievable run times of about $500M$ are roughly 10 times larger than for singularity avoiding slicings, we have found that introducing an artificial asymmetry on the full grid by simply off-setting the excision box one grid point in all directions makes the runs fail much sooner. Although the slope of the blow-up is not significantly affected when this artificial asymmetry is introduced, the exponential growth becomes evident from the very beginning. On the other hand, the full grid runs can be stabilized by setting certain terms in the BSSN equations to their analytic values. In particular, freezing the evolution of the $\tilde{\Gamma}^i$ while keeping the shift static suffices to obtain stability. In conclusion, the instability appears to be more directly linked to the system of evolution equations than to the boundary condition, and we will investigate different variations of the evolution system in the future.

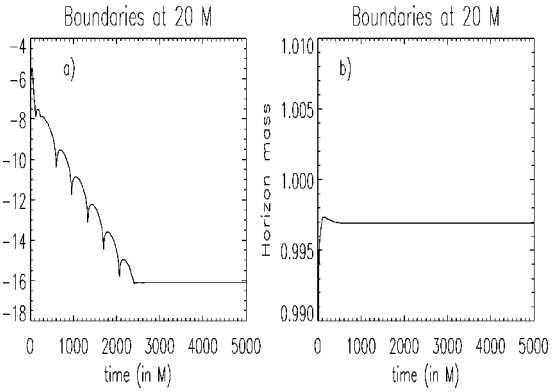

FIG. 6. Simulation using Gamma driver shift with $k=0.1$; $\Delta x=0.4$, $\Delta t=0.1$, 53^3 points, boundary at $20M$. (a) Log plot of rms of change in the lapse. (b) Horizon mass.

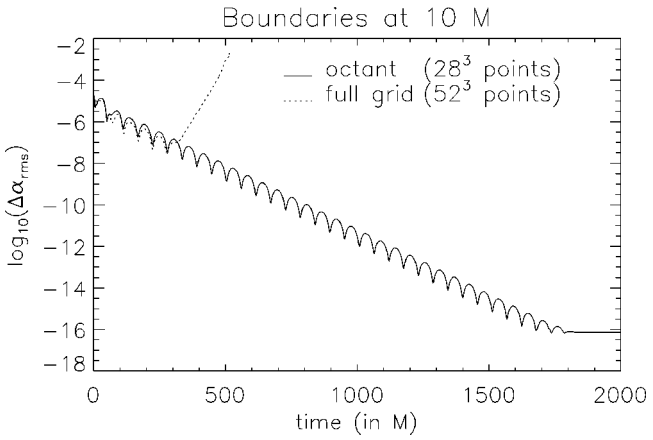

FIG. 7. Unstable mode on a full grid for $1+\log$ slicing with a static shift. Shown is a log plot of the rms of the change in the lapse for an octant run with $\Delta x=0.4$, $\Delta t=0.1$, and 28^3 grid points together with the corresponding full grid run.

We have also repeated the above simulations using the ADM equations with the same gauge and boundary conditions, and the same numerical techniques, but these runs fail already at $t\simeq 30M$ even in octant mode.

V. CONCLUSIONS

We have described a black hole excision technique in 3+1 numerical relativity that has allowed us to obtain accu-

rate, long-term stable evolutions of black hole spacetime in 3D. The main limitation is that the transition from octant symmetry to full grids introduces an unstable mode, which is currently under investigation. Our implementation of excision is based on the idea of simplifying all ingredients of the excision algorithm as much as possible. In our case this means (1) excising a cube naturally adapted to the underlying Cartesian coordinates, (2) imposing a simple but stable boundary condition on the sides of this cube, and (3) using an upwind scheme instead of causal differencing. Crucial for obtaining our long-term stable evolutions has been the use of a live slicing condition and a radiation outer boundary condition. Although keeping a static shift does not appear to have a detrimental effect on the stability of our simulations, we have also experimented with several live shift conditions, both algebraic and elliptic, that can be generalized to more interesting physical situations. We consider these results a necessary first step towards the development of excision techniques capable of evolving the full inspiral collision of two black holes in an accurate and stable way.

ACKNOWLEDGMENTS

We would like to thank J. Baker, D. Pollney, E. Seidel, W.-M. Suen and J. Thornburg for useful discussions and comments. The numerical experiments were implemented using BAM and the Cactus Computational Toolkit [39,40]. All computations were performed at the Max-Planck-Institut für Gravitationsphysik.

[1] E. Seidel and W.-M. Suen, Phys. Rev. Lett. **69**, 1845 (1992).
[2] P. Anninos *et al.*, Phys. Rev. D **51**, 5562 (1995).
[3] J. Thornburg, Class. Quantum Grav. **4**, 1119 (1987).
[4] J. Thornburg, Ph.D. thesis, University of British Columbia, Vancouver, British Columbia, 1993.
[5] M. A. Scheel, S. L. Shapiro, and S. A. Teukolsky, Phys. Rev. D **51**, 4208 (1995).
[6] R. Marsa and M. Choptuik, Phys. Rev. D **54**, 4929 (1996).
[7] C. Gundlach and P. Walker, Class. Quantum Grav. **16**, 991 (1999).
[8] M. Scheel *et al.*, Phys. Rev. D **56**, 6320 (1997).
[9] M. A. Scheel *et al.*, Phys. Rev. D **58**, 044020 (1998).
[10] L. E. Kidder *et al.*, Phys. Rev. D **62**, 084032 (2000).
[11] P. Anninos *et al.*, Phys. Rev. D **52**, 2059 (1995).
[12] G. E. Daues, Ph.D. thesis, Washington University, St. Louis, Missouri, 1996.
[13] B. Brügmann, Phys. Rev. D **54**, 7361 (1996).
[14] P. Walker, Ph.D. thesis, University of Illinois at Urbana-Champaign, Urbana, Illinois, 1998.
[15] G. B. Cook *et al.*, Phys. Rev. Lett. **80**, 2512 (1998).
[16] J. Thronburg, gr-qc/9906022.
[17] R. Gomez *et al.*, Phys. Rev. Lett. **80**, 3915 (1998).
[18] M. Alcubierre and B. Schutz, J. Comput. Phys. **112**, 44 (1994).
[19] C. W. Misner, K. S. Thorne, and J. A. Wheeler, *Gravitation* (Freeman, San Francisco, 1973).
[20] T. W. Baumgarte and S. L. Shapiro, Phys. Rev. D **59**, 024007 (1999).
[21] M. Shibata and T. Nakamura, Phys. Rev. D **52**, 5428 (1995).
[22] R. Arnowitt, S. Deser, and C. W. Misner, in *Gravitation: An Introduction to Current Research*, edited by L. Witten (Wiley, New York, 1962), pp. 227–265.
[23] T. W. Baumgarte, S. A. Hughes, and S. L. Shapiro, gr-qc/9902024.
[24] M. Shibata, Phys. Rev. D **60**, 104052 (1999).
[25] M. Shibata and K. Uryu, Phys. Rev. D **61**, 064001 (2000).
[26] M. Shibata, T. W. Baumgarte, and S. L. Shapiro, Phys. Rev. D **61**, 044012 (2000).
[27] M. Alcubierre *et al.*, Phys. Rev. D **61**, 041501 (2000).
[28] M. Alcubierre *et al.*, Phys. Rev. D **62**, 124011 (2000).
[29] M. Alcubierre *et al.*, Phys. Rev. D **62**, 044034 (2000).
[30] C. Bona, J. Massó, E. Seidel, and J. Stela, Phys. Rev. Lett. **75**, 600 (1995).
[31] L. Smarr and J. York, Phys. Rev. D **17**, 2529 (1978).
[32] L. Smarr and J. York, Phys. Rev. D **17**, 1945 (1978).
[33] L. Andersson and V. Moncrief (unpublished).
[34] B. Brügmann, Int. J. Mod. Phys. D **8**, 85 (1999).
[35] J. Balakrishna *et al.*, Class. Quantum Grav. **13**, L135 (1996).
[36] H. Friedrich and G. Nagy, Commun. Math. Phys. **201**, 619 (1999).
[37] A. Arbona, C. Bona, J. Massó, and J. Stela, Phys. Rev. D **60**, 104014 (1999).
[38] M. Alcubierre *et al.*, Class. Quantum Grav. **17**, 2159 (2000).
[39] B. Brügmann, Ann. Phys. (Leipzig) **9**, 227 (2000).
[40] http://www.cactuscode.org